E2-2002-116

G. N. Afanasiev[1], V. M. Shilov, Yu. P. Stepanovsky[2]

ANALYTICAL TREATMENT OF THE SMOOTHED TAMM PROBLEM

Submitted to «Journal of Physics A»

[1]E-mail: afanasev@thsun1.jinr.ru
[2]Institute of Physics and Technology, Kharkov, Ukraine

Афанасьев Г. Н., Шилов В. М., Степановский Ю. П. E2-2002-116
Аналитическое рассмотрение сглаженной задачи Тамма

Рассматривается движение заряда в среде на конечном интервале. Для движения, описываемого абсолютно непрерывными функциями времени (это означает, что скорость заряда и все ее производные по времени являются непрерывными функциями), интенсивность излучения при скорости заряда v, большей скорости света в веществе c_n, пропорциональна частоте в определенном интервале углов и убывает экспоненциально вне этого интервала. Для движения заряда со скачками ускорения, но без скачков скорости экспоненциальное убывание сменяется $1/\omega$ -убыванием. Для замедленного движения, когда начальная и конечная скорости заряда превышают c_n, угловая интенсивность излучения содержит плато. В практически важном случае, соответствующем полной остановке заряда, интенсивность излучения максимальна при черенковском угле θ_c, соответствующем начальной скорости, и быстро убывает при $\theta > \theta_c$. Интегральная интенсивность (полученная интегрированием по телесному углу), соответствующая этому движению, является линейной функцией частоты (несмотря на сильное нарушение условия Тамма), если скорость заряда превышает c_n.

Работа выполнена в Лаборатории теоретической физики им. Н. Н. Боголюбова ОИЯИ.

Препринт Объединенного института ядерных исследований. Дубна, 2002

Afanasiev G. N., Shilov V. M., Stepanovsky Yu. P. E2-2002-116
Analytical Treatment of the Smoothed Tamm Problem

The charge motion in medium in a finite space interval is considered. For the motion described by absolutely continuous functions of time (this means that the charge velocity and all its time derivatives are also continuous), the radiation intensity, for the charge velocity v greater than the light velocity in medium c_n, is proportional to frequency in some angular region and exponentially decreases outside it. For the motion without velocity jumps, but with acceleration ones, the exponential decrease changes by the $1/\omega$ one. For the pure decelerated motion, when both initial and final velocities are greater than c_n, the radiation intensity contains a plato. In a practically important case corresponding to the zero final charge velocity, the radiation intensity is maximal at the Cherenkov angle θ_c corresponding to the initial charge velocity and sharply decreases for $\theta > \theta_c$. The integral intensity (obtained by integration of the angular radiation intensity over the solid angle) corresponding to this motion is a linear function of the frequency (despite the strong violation of the Tamm condition) when the charge velocity exceeds c_n.

The investigation has been performed at the Bogoliubov Laboratory of Theoretical Physics, JINR.

Preprint of the Joint Institute for Nuclear Research. Dubna, 2002

1 Introduction

The aim of this consideration is to study the properties of the so-called smoothed Tamm problem. The original Tamm problem [1] deals with a charge instantly accelerated at the start of motion, uniformly moving on a finite space interval and instantly decelerated at the end of motion. Under some approximations (see below), Tamm obtained the remarkably simple formula describing the intensity of radiation:

$$\sigma_T(\theta,\omega) = \frac{e^2\sin^2\theta}{\pi^2 nc}[\frac{\sin k_n z_0(\cos\theta - 1/\beta_n)}{\cos\theta - 1/\beta_n}]^2. \qquad (1.1)$$

Here θ is the observation angle counted from the motion axis, n is the medium refractive index ($n = \sqrt{\epsilon\mu}$), $\beta_n = \beta n$, $\beta = v/c$, v is the charge velocity, $k_n = kn$, $k = \omega/c = 2\pi/\lambda$ is the wave number, and $z_0 = L/2$ (L is the motion interval).
There are two different interpretations of this formula. Tamm and Frank associated it with the radiation of a charge moving uniformly on a finite space interval. On the other hand, Vavilov [2] attributed the radiation observed in Cherenkov experiments to the charge deceleration arising from the ionization energy losses. Later, Ruzicka and Zrelov [3,4], associated (1.1) with the interference of two bremsstrahlung (BS) shock waves arising at the start and end of motion. In order not to be involved into this dispute, we consider analytically and numerically the so-called smoothed Tamm problem in which the charge velocity varies smoothly, without jumps. Since there are no infinite accelerations in nature, the smoothed Tamm problem may be viewed as a suitable, quite useful for experimentalists, idealization.

The plan of our exposition is as follows. The treated motion laws are discussed in Section 2. The necessary mathematical formulae and the approximations used are presented in Section 3. In Section 4, we give without derivation the analytical radiation intensities corresponding to a charge moving in medium with the motion laws treated in Section 2. Various limiting cases are also considered. Numerical calculations supporting analytic results of the previous section are collected in Section 5. Finally, in Section 6, we give a short discussion of the results obtained.

2 Treated motion laws

The following charge motions in medium will be considered:

1. A charge, being initially ($t < -t_0$) at the state of rest at the point $z = -z_0$, in the space-time interval ($-t_0 < t < -t_1, \quad -z_0 < z < -z_1$) moves with a constant acceleration up to acquiring the velocity v_0 with which it moves in the space-time interval ($-t_1 < t < t_1, \quad -z_1 < z < z_1$). After that ($t_1 < t < t_0, \quad z_1 < z < z_0$), a charge is uniformly decelerated up to reaching the state of rest at the point $z = z_0$ (Fig. 1).

2. A charge moves according to the law (Fig. 2)

$$v(t) = \frac{v_0}{\cosh^2(t/t_0)}. \tag{2.1}$$

Obviously, $v(t) = v_0$ for $t = 0$ and $v(t) \to 0$ for $t \to \pm\infty$. The charge position at the moment t is given by $z(t) = v_0 t_0 \tanh(t/t_0)$. Therefore, the charge motion is confined to $-L/2 < z < L/2$, where $L = 2v_0t_0$ is the motion interval. The velocity, being expressed through the current charge position, is

$$v(z) = v_0(1 - 4z^2/L^2) \tag{2.2}$$

The drawback of this motion is that one can not change t_0 without changing the motion interval L.

3. A charge moves according to the law (Fig. 3)

$$v = \frac{1}{2}v_0(\tanh\frac{t+T_0}{T} - \tanh\frac{t-T_0}{T}), \tag{2.3}$$

The maximal velocity (at $t = 0$) is $\tilde{v}_0 = v_0 \tanh(T_0/T)$. Equation (2.3) is slightly inconvenient. When we change either T or T_0, the maximal velocity, the interval to which the motion is confined, and the behaviour of the velocity inside this interval are also changed. We rewrite this expression in a slightly different form, more suitable for applications

$$v(t) = \tilde{v}_0\frac{1 + \cosh(2T_0/T)}{\cosh(2t/T) + \cosh(2T_0/T)}, \tag{2.4}$$

The charge position at the moment t is given by

$$z(t) = \frac{LT}{4T_0}\ln\frac{\cosh(t+T_0)/T}{\cosh(t-T_0)/T}, \tag{2.5}$$

where

$$L = 2v_0T_0 = 2\tilde{v}_0T_0\coth(T_0/T) \tag{2.6}$$

is the motion interval. We reverse this expression, thus obtaining

$$\frac{T_0}{T} = \frac{1}{2}\ln\frac{1 + 2T_0\tilde{v}_0/L}{1 - 2T_0\tilde{v}_0/L}. \tag{2.7}$$

It is seen that the fixing of $\tilde{v}_0$ and L leaves only one free parameter. If we identify it with T_0, then (2.7) defines T as a function of T_0 (for the fixed L and $\tilde{v}_0$). For $T_0 << T$, the r.h.s. of (2.7) should also be small. This is possible if $2T_0\tilde{v}_0/L << 1$. Then, r.h.s. of (2.7) tends to $2T_0\tilde{v}_0/L$. Equating both sides of (2.7), we find that $T = L/2\tilde{v}_0$ in this limit. For $T_0 \to L/2\tilde{v}_0$ the r.h.s. of (2.7) tends to ∞. Therefore, $T/T_0 \to 0$. It follows from this that the available interval for T and T_0 is $(0, L/2\tilde{v}_0)$

(for the fixed L and $\tilde{v}_0$). We express the charge velocity through its current position z. For this, we at first express $\cosh(2t/T)$ through z:

$$\cosh\frac{2t}{T}=\frac{\sinh[T_0(1+2z/L)/T]}{2\sinh[T_0(1-2z/L)/T]}+\frac{\sinh[T_0(1-2z/L)/T]}{2\sinh[T_0(1+2z/L)/T]}. \tag{2.8}$$

Substituting this into (2.4), we obtain $v(z)$. For $T_0 << T$, $v(z)$ reduces to

$$v(z)=\tilde{v}_0(1-\frac{4z^2}{L^2}), \tag{2.9}$$

which coincides with (2.2) if we identify $\tilde{v}_0$ with v_0. In the opposite case ($T << T_0$),

$$v(z)=\frac{\tilde{v}_0}{1+\exp(-2T_0/T)\cosh(2t/T)}. \tag{2.10}$$

If z is so close to $(L/2)$, that

$$1-\frac{2z}{L}<<\frac{T}{T_0},$$

then (2.8) gives

$$\cosh\frac{2t}{T}=\frac{2T_0}{T}(1-\frac{2z}{L})\exp(\frac{2T_0}{T}) \quad \text{and} \quad v(z)=\frac{2\tilde{v}_0T_0}{T}(1-\frac{2z}{L}). \tag{2.11}$$

On the other hand, if

$$1-\frac{2z}{L}>>\frac{T}{T_0},$$

then

$$\cosh(2t/T)=1 \quad \text{and} \quad v=\tilde{v}_0. \tag{2.12}$$

Since, according to our assumption, $T/T_0 << 1$, the transition from (2.11) to (2.12) is realized in a very narrow z interval. For example, for $T/T_0=10^{-6}$, it takes place in the interval $(1-10^{-5})<2z/L<(1-10^{-7})$. The same considerations are valid in the neigbourhood of another boundary point $z=-L/2$.

We conclude: the horizontal part (where $v\approx\tilde{v}_0$) of the charge trajectory exists if $T << T_0$ (see (2.12)) and does not exist if $T_0 << T$ (see (2.9)). However, in both cases ($T << T_0$ and $T >> T_0$), $v(z)$ decreases linearly when z approaches boundary points. The motion law (2.4) is much richer than (2.1). It is extensively used in nuclear physics to parametrize the nuclear densities [5,6].

4. Let a charge move in the (z_1, z_2) interval according to the motion law (Fig. 4):

$$z=z_1+v_1(t-t_1)+\frac{1}{2}a(t-t_1)^2. \tag{2.13}$$

The motion begins at the moment t_1 at the space point z_1 and terminates at the moment t_2 at the space point z_2. A charge is at rest for $t_1<0$ and $t_2>0$. The

charge velocity varies linearly with time from the value $v = v_1$ at $t = t_1$ up (or down) to value $v = v_2$ at $t = t_2$: $v = v_1 + a(t - t_1)$. The acceleration a and the time motion interval can be expressed through z_1, z_2, v_1, v_2:

$$a = \frac{v_1^2 - v_2^2}{2(z_1 - z_2)}, \quad t_2 - t_1 = \frac{2(z_2 - z_1)}{v_2 + v_1}.$$

A particular interesting case having numerous practical applications corresponds to the complete termination of motion ($\beta_2 = 0$).

5. Let a charge moves according to the law (Fig. 5)

$$v = v_+ + v_- \tanh \frac{t}{t_0}, \quad v_\pm = \frac{v_1 \pm v_2}{2}, \quad -\infty < t < \infty. \tag{2.14}$$

The current charge position is $z = v_+ t + v_- t_0 \ln \cosh(t/t_0)$. For $t \to \pm\infty$, $v \to v_{1,2}$ and $z \to v_{1,2} t$.
Formerly, exact radiation intensities for the motion laws (2.1),(2.2) and (2.14) were obtained in Refs. [7-10] for a charge moving in vacuum. It was shown there that angular-frequency radiation intensities are exponentially small at large frequencies. It will be shown below that, in the presence of matter, the asymptotic behaviour changes dramaticaly: their exponential decrease disappears in some interval of velocities and angles changing by the linear rise with ω.

3 Necessary mathematical formulae and approximations

Consider a point-like charge moving in medium with parameters ϵ and μ. Let the charge velocity and trajectory be $\vec{v}(t)$ and $\vec{\xi}(t)$. For the definiteness, let it move along the z axis. The magnetic vector potential (only its z component differs from sero) corresponding to this motion is

$$A_\omega = \frac{\mu e}{2\pi c} \int \frac{1}{R} \exp[i\omega(t' + R/c_n)] j(t') dt', \tag{3.1}$$

where $R = [\rho^2 + (z - \xi)^2]^{1/2}, \xi = z(t')$, and $c_n = c/n$ is the light velocity in medium. Differentiating this expression, one finds electromagnetic field strengths and the energy flux through the observation sphere S of the radius r per unit frequency and per unit solid angle

$$\sigma_r(\theta, \omega) = \frac{d^2\mathcal{E}}{d\omega\Omega} = \frac{e^2 \mu n k^2 \sin^2\theta}{4\pi^2 c} (I_c I_c' + I_s I_s'), \tag{3.2}$$

where

$$I_c = \int \frac{v dt'}{R^2} (\cos\psi - \frac{\sin\psi}{k_n r R}), \quad I_s = \int \frac{v dt'}{R^2} (\sin\psi + \frac{1}{k_n R r} \cos\psi),$$

$$I'_c = \int \frac{vdt'}{R^3}(1 - \frac{\xi}{r}\cos\theta)(\cos\psi - 3\frac{\sin\psi}{k_n Rr} - 3\frac{\cos\psi}{k_n^2 R^2 r^2}),$$

$$I'_s = \int \frac{vdt'}{R^3}(1 - \frac{\xi}{r}\cos\theta)(\sin\psi + 3\frac{\cos\psi}{k_n Rr} - 3\frac{\sin\psi}{k_n^2 r^2 R^2}),$$

$$\psi = \omega t' + k_n r(R-1), \quad R = [1 + \frac{\xi^2}{r^2} - 2\frac{\xi}{r}\cos\theta]^{1/2}, \quad k_n = kn,$$

r and θ define radial and angular positions of the observation point, and $n = \sqrt{\epsilon\mu}$ is the medium refractive index. When obtaining (3.2), it is implicitly suggested that the charge motion interval lies entirely inside the observation sphere S.

However, Eq. (3.2) is not suitable for practical applications and the qualitative analysis of radiation intensities. Therefore, some approximations are needed. We briefly enumerate them:

1. In the wave zone, where $kr >> 1$, one can disregard terms of the order $1/kr$ and higher, thus obtaining

$$I_c = \int \frac{vdt'}{R^2}\cos\psi, \quad I_s = \int \frac{vdt'}{R^2}\sin\psi,$$

$$I'_c = \int \frac{vdt'}{R^3}(1 - \frac{\xi}{r}\cos\theta)\cos\psi, \quad I'_s = \int \frac{vdt'}{R^3}(1 - \frac{\xi}{r}\cos\theta)\sin\psi.$$

Usually, this approximation is satisfied with a great accuracy. For the observation sphere radius $r = 1m$ and the wavelength $\lambda = 4 \cdot 10^{-5} cm$, kr is about 10^7.

2. When the observation sphere radius r is much larger than the motion interval, one can disregard the ratio ξ/r everywhere except for the ψ function. Then,

$$I_c = I'_c = \int vdt'\cos\psi, \quad I_s = I'_s = \int vdt'\sin\psi \quad \text{and}$$

$$\sigma_r(\theta,\omega) = \frac{d^2\mathcal{E}}{d\omega\Omega} = \frac{e^2\mu n k^2 \sin^2\theta}{4\pi^2 c}[(I_c)^2 + (I_s)^2]. \tag{3.3}$$

Usually, this condition is fulfilled in a majority of experiments.

3. The most serious approximation is $kL^2/r << 1$ (L is the motion interval). It arises from the fact that the development of the $k_n r(R-1)$ term entering in ψ has the form

$$k_n r(R-1) = -k_n\xi\cos\theta + \frac{k_n\xi^2\sin^2\theta}{2r} + \ldots \quad .$$

The Tamm approximation is obtained when the last term in this expression is neglected. This is possible, if it is much smaller than π (since ψ enters into sines and cosines). Then, ψ takes the form

$$\psi = \omega t' - kn\xi(t')\cos\theta. \tag{3.4}$$

In realistic conditions, this approximation is not satisfied. For example, for $\lambda = 4 \cdot 10^{-5} cm$, $L = 1cm$ and $r = 1m$, the discussed condition reduces to $400 << 1$, that is, it is greatly violated. The complications arising from the radiation intensity measurements at finite distances and the analytic formulae removing the above drawbacks were discussed in [11,12]. When the conditions 1-3 are fulfilled, the vector potential (3.1) reduces to

$$A_\omega = \frac{\mu e}{2\pi cr} \exp(iknr) I, \tag{3.5}$$

where

$$I = \int v(t') \exp[i(\omega t' - kn \cos\theta z(t'))] dt'.$$

Electromagnetic field strengths contributing to the radial energy flux are

$$H_\phi = -\frac{ienk \sin\theta}{2\pi cr} \exp(iknr) I, \quad E_\theta = -\frac{iemk \sin\theta}{2\pi cr} \exp(iknr) I.$$

The radiation intensity is given by

$$\sigma_r(\theta, \omega) = \frac{d^2\mathcal{E}}{d\omega d\Omega} = \frac{e^2 k^2 n \mu}{4\pi^2 c} \sin^2\theta |I|^2. \tag{3.6}$$

This means that all information on the radiation intensity is contained in I. In the quasiclassical approximation,

$$I = v(t_c) \sqrt{\frac{2\pi}{|\dot{v}(t_c) kn \cos\theta|}} \exp(\pm i\pi/4) \exp(i\psi_c), \tag{3.7}$$

where $\psi_c = \omega t_c - knz_c \cos\theta$, $z_c = z(t_c)$ and t_c is found from the equation

$$1 - n\beta(t_c) \cos\theta = 0. \tag{3.8}$$

The $\pm$ signs in (3.7) coincide with the the sign of $\dot{v}(t_c) kn \cos\theta$. Under the conditions (1-3), the charge uniformly moving in the interval $(-z_0, z_0)$ radiates with the intensity given by the famous Tamm formula (1.1). As an example, in Fig. 6 we present the Tamm radiation intensity and the one corresponding to the finite observation distance and evaluated via (3.2). We see in this figure a plato in the neighbourhood of the Cherenkov angle θ_c ($\cos\theta_c = 1/\beta n$). Its origin is due to the fact that, in the Tamm problem, a charge moving in a finite space interval L, emits Cherenkov radiation from each point of its path. These particular radiations, being combined, form the Cherenkov shock wave of a finite extension propagating at the angle θ_c towards the motion axis and intersecting the observation sphere S of the radius R in the angle interval $\Delta\theta = \sqrt{1 - 1/\beta^2 n^2 L/r} \approx 4.2^0$ for the observation parameters the same as in Fig. 1. These questions were considered in detail in [13].

The aim of this consideration is to investigate the deviation from the Tamm formula (corresponding to the instantaneous acceleration and deceleration at the start and end of motion, resp.) associated with smooth acceleration and deceleration of a charged particle. Although the evaluation via (3.2) takes into account finite distances effects, but it obscures the acceleration effects, which we intend to study here. For this reason, we shall deliberately use (3.3) with ψ given by (3.4).

4 Analytic estimates

4.1 Superposition of uniform and accelerated motions

For the motion shown in Fig.1, the exact solution in terms of Fresnel integrals was found in [14]. We give only the final result. We should evaluate the integrals $I_c = \int v dt' \cos\psi$ and $I_s = \int v dt' \sin\psi$ entering into (3.3). For ψ in the form (3.4), I_s=0 due to the symmetry of the treated problem. Then, I_c reduces to

$$I_c = I_c^a + I_c^d + I_c^u = 2I_c^a + I_c^u, \tag{4.1}$$

where I_c^a, I_c^d, and I_c^u are integrals over the accelerated ($-z_0 < z < -z_1$), decelerated ($z_1 < z < z_0$) and uniform ($-z_1 < z < z_1$) parts of a charge trajectory, respectively. Again, it was taken into account that $I_c^a = I_c^d$ due to the symmetry of the problem. The integral I_c^u describing the uniform motion on the interval ($-z_1 < z < z_1$) is

$$I_c^u = \frac{2\beta}{k(1-\beta n\cos\theta)} \sin[\frac{kz_1}{\beta}(1-\beta n\cos\theta)]. \tag{4.2}$$

Then, for $\theta < \pi/2$, one gets [14]

$$I_c^a = \int\limits_{-z_0}^{-z_1} dz \cos\psi = \frac{1}{kn\cos\theta}\{\sin(u_2^2-\gamma) - \sin(u_1^2-\gamma) +$$

$$\alpha\sqrt{2\pi}[\cos\gamma(C_2-C_1) + \sin\gamma(S_2-S_1)]\}, \tag{4.3}$$

where we put $C_1 = C(u_1)$, $C_2 = C(u_2)$, $S_1 = S(u_1)$, $S_2 = S(u_2)$; C and S are the Fresnel integrals defined as

$$S(x) = \sqrt{\frac{2}{\pi}} \int\limits_0^x dt \sin t^2 \quad \text{and} \quad C(x) = \sqrt{\frac{2}{\pi}} \int\limits_0^x dt \cos t^2.$$

For the treated motion, u_1, u_2, α, and γ are given by

$$u_1 = -\sqrt{k(z_0-z_1)n\cos\theta}\frac{1}{\beta n\cos\theta}, \quad u_2 = \sqrt{k(z_0-z_1)n\cos\theta}(1-\frac{1}{\beta n\cos\theta}),$$

$$\alpha = \frac{1}{\beta}[\frac{k(z_0-z_1)}{n\cos\theta}]^{1/2}, \quad \gamma = kz_0 n\cos\theta + \frac{k(z_0-z_1)}{\beta^2 n\cos\theta} - \frac{k(2z_0-z_1)}{\beta}.$$

Consider the limiting cases.

When $k(z_0-z_1) << 1$ (the accelerated motion interval is much smaller than the observed wavelength), $I_c^a = I_c^d \approx 0$ (despite the infinite acceleration in this limit), and the radiation intensity coincides with the Tamm one.

In the opposite case ($k(z_0 - z_1) >> 1$), one can change Fresnel integrals by their asymptotic values. Then, for $\theta < \theta_c$ ($\cos\theta_c = 1/\beta n$) one gets

$$I_c^a = -\alpha\sqrt{2\pi}\frac{\cos\gamma + \sin\gamma}{kn\cos\theta} + \frac{\beta n}{k(\beta n\cos\theta - 1)}\sin[kz_1(1 - \beta n\cos\theta)]. \tag{4.4}$$

To obtain I_c, one should double I_c^a (since $I_c^a = I_c^d$) and add I_c^u given by (4.2). This gives

$$I_c = 2I_c^a + I_c^u = -\alpha\sqrt{2\pi}\frac{\cos\gamma + \sin\gamma}{kn\cos\theta} \quad \text{and}$$

$$\sigma_r = \frac{e^2}{2\pi cn^2\beta^2}k(z_0 - z_1)\frac{\sin^2\theta}{\cos^3\theta}(1 + \sin 2\gamma). \tag{4.5}$$

In this angular region, the oscillations are due to the $(1+\sin 2\gamma)$ factor. The maximal value of σ_r is very large (due to the $k(z_0 - z_1) >> 1$ factor). On the other hand, for $\theta > \theta_c$, one obtains

$$I_c^a = \frac{\beta n}{k(\beta n\cos\theta - 1)}\sin[kz_1(1 - \beta n\cos\theta)]. \tag{4.6}$$

This expression is valid for all θ if $\beta n < 1$. Inserting (4.2) and (4.6) into (4.1), one finds

$$I_c = 2I_c^a + I_c^u = 0.$$

We see that for $\theta > \theta_c$ the summary contribution of the accelerated and decelerated parts of the charge trajectory is compensated by the contribution of its uniform part. The next order terms arising from the asymptotic expansion of the Fresnel integrals are of the order $1/k(z_0 - z_1)$ and, therefore, are negligible for $k(z_0 - z_1) >> 1$.

For $\theta > \theta_c$, the radiation intensity disappears for arbitrary z_1 satisfying the conditon $k(z_0 - z_1) >> 1$ and, in particular, for $z_1 = 0$. In this case, there is no uniform motion, and accelerated motion in the interval $-z_0 < z < 0$ is followed by the decelerated motion in the interval $0 < z < z_0$. The radiation intensity is obtained from (4.3) by putting $z_1 = 0$ in it. For $kz_0 >> 1$ it reduces to

$$\sigma_r = \frac{e^2 kz_0\sin^2\theta}{2\pi n^2 c\cos^3\theta}(1 + \sin 2\gamma) \tag{4.7}$$

for $\theta < \theta_c$. Here $\gamma = (1 - 1/\beta n\cos\theta)^2 kz_0 n\cos\theta$. For $\theta > \theta_c$, σ_r is of the order $1/kz_0$. Due to the $(1 + \sin 2\gamma)$ factor, σ_r for $\theta < \theta_c$ is a fastly oscillating function of θ with a large amplitude (since $kz_0 >> 1$). For $\beta n < 1$, the condition $\theta < \theta_c$ cannot be satisfied and radiation intensities are of the order $1/k(z_0 - z_1) << 1$ for all angles. In the opposite case ($kz_0 \to 0$), the radiation intensity tends to zero:

$$\sigma_r = \frac{e^2\mu nk^2 z_0^2\sin^2\theta}{\pi^2 c}. \tag{4.8}$$

This particular case indicates that the disappearance of radiation intensities for high frequencies above some critical angle has a more general reason. It will be shown in

the next two subsections that radiation intensities describing the absolutely continuous charge motion in medium are exponentially small outside some angular region. It should be stressed that formulae obtained in this section are not valid near the angle θ_c where the arguments of the Fresnel integrals vanish.

In the time representation, the charge motion shown in Fig. 1 was considered in [15]. It was shown there that at the moment when the charge velocity coincides with the light velocity in medium c_n (in the time interval $-t_0 < t < -t_1$), the complex arises consisting of the Cherenkov shock wave and the shock wave closing the Cherenkov cone and not coinciding with the bremsstrahlung shock wave. As time goes, the dimensions of this complex grow. At the moment when the charge velocity again coincides with c_n (in the time interval $t_1 < t < t_0$), the above complex detaches from a charge and propagates with the light velocity in medium. The content of this section may be viewed as a translation of [15] into the frequency language (which is more frequently used by experimentalists).

4.2 The motion law (2.1)

For the motion law shown in Fig. 2, the amplitude I is given by

$$I = \frac{\pi v_0 \omega t_0^2}{\sinh(\pi\omega t_0/2)} \exp(i\omega t_0 \beta_0 n \cos\theta) \Phi(1 + i\omega t_0/2; 2; -2i\omega t_0 \beta_0 n \cos\theta),$$

where $\Phi(\alpha; \beta; z)$ is the confluent hypergeometric function. Correspondingly, the radiation intensity is

$$\sigma_r(\theta, \omega) = \frac{e^2 n \mu \beta_0^2 \omega^4 t_0^4}{4c \sinh^2(\pi\omega t_0/2)} |\Phi|^2. \tag{4.9}$$

When $\omega t_0 << 1$,

$$I = 2v_0 t_0 \quad \text{and} \quad \sigma_r(\theta, \omega) = \frac{n\mu}{\pi^2 c} e^2 \beta_0^2 \omega^2 t_0^2 \sin^2\theta. \tag{4.10}$$

This coincides with (4.8). In the opposite case ($\omega t_0 >> 1$), by applying the quasiclassical approximation, one finds that I is exponentially small for all angles if $\beta_0 < 1/n$. If $\beta_0 > 1/n$, I is exponentially small for $\theta > \theta_c$ ($\cos\theta_c = 1/\beta_0 n$) and

$$|I|^2 = \frac{\pi c t_0 \sqrt{\beta_0}}{(n\cos\theta)^{3/2} k (\beta_0 n \cos\theta - 1)^{1/2}} \cos^2\psi_c \tag{4.11}$$

for $\theta < \theta_c$. Here

$$\psi_c = \omega(t_c - \frac{n z_c}{c}\cos\theta) + \frac{\pi}{4}, \quad \cosh\frac{t_c}{t_0} = \sqrt{\beta_0 n \cos\theta}, \quad z_c = v_0 t_0 (1 - \frac{1}{n\beta_0\cos\theta})^{1/2}.$$

When evaluating $|I|^2$, it was taken into account that Eq. (3.8) has two real roots for $\beta_0 n > 1$:

$$t_c = \pm t_0 (\sqrt{\beta_0 n \cos\theta} + \sqrt{\beta_0 n \cos\theta - 1}).$$

The radiation intensity (3.6), with $|I|^2$ given by (4.11), is the analogue of the Tamm formula (1.1) for the motion law (2.1).

Formerly, analytical radiation intensities for the charge motion in vacuum shown in Fig.2, were obtained in [7]. In this case, (3.8) has no real roots and, at high frequencies, the quasiclassical radiation intensity is exponentially small for all angles.

4.3 The motion law (2.2)

For the motion law shown in Fig.3, the amplitude I equals

$$I = \frac{1}{2} v_0 T \exp[-i\omega T_0(1-\beta_0 n\cos\theta)] \frac{\omega\pi T/2}{\sinh(\omega\pi T/2)} [1-\exp(-4T_0/T)]\times$$

$$ {}_2F_1[1-\frac{i\omega T}{2}\beta_0 n\cos\theta, 1+\frac{i\omega T}{2}; 2; 1-\exp(-4T_0/T)]. \qquad (4.12)$$

Here ${}_2F_1(\alpha,\beta;\gamma;z)$ is the usual hypergeometric function. The radiation intensity is

$$\sigma_r(\theta,\omega) = \frac{e^2\mu n\beta_0^2\omega^4 T^4\sin^2\theta}{64c\sinh^2(\pi\omega T/2)}[1-\exp(-4T_0/T)]^2|F|^2. \qquad (4.13)$$

Consider particular cases:
Let T be much smaller than T_0 (ωT is arbitrary). Then,

$$\sigma_r = \frac{e^2\mu\beta_0\omega T\sin^2\theta}{8\pi^3 c\cos\theta(n\beta_0\cos\theta-1)} \frac{\sinh[(\pi\omega T n\beta_0\cos\theta)/2]}{\sinh(\pi\omega T/2)\sinh[\pi\omega T(\beta_0 n\cos\theta-1)/2]}. \qquad (4.14)$$

If, in addition, the frequency is so large that $\omega T >> 1$, then (4.14), for $\beta_0 n < 1$, is exponentially small for all angles:

$$\sigma_r = \frac{e^2\mu\beta_0\omega T}{4\pi^3 c\cos\theta(1-n\beta_0\cos\theta)}\sin^2\theta\exp[-\pi\omega T(1-n\beta_0\cos\theta)]. \qquad (4.15)$$

For $\beta_0 n > 1$ and $\theta > \theta_c$, $(\cos\theta_c = 1/\beta_0 n)$, the radiation intensity (4.14) coincides with (4.15). On the other hand, for $\theta < \theta_c$

$$\sigma_r = \frac{e^2\mu\beta_0\omega T}{4\pi^3 c\cos\theta(n\beta_0\cos\theta-1)}\sin^2\theta. \qquad (4.16)$$

In this case there is no exponential damping.
Let T_0 be much smaller than T. We should at first express v_0 through $\tilde{v}_0$ and then take the limit $T_0/T \to 0$. Then, the hypergeometric function ${}_2F_1$ entering into (4.12) is transformed into the confluent hypergeometric function Φ entering into (4.8), and (4.13) is transformed into (4.9) if we identify T and $\tilde{v}_0$ entering into (4.13) (after expessing v_0 through $\tilde{v}_0$) with t_0 and v_0 entering into (4.9).
In the limit $\omega T \to 0$, (4.13) goes into

$$\sigma_r = \frac{e^2\mu n\beta_0^2\omega^2 T_0^2}{\pi^2 c}\sin^2\theta,$$

which coincides with (4.8) and (4.10). The quasiclassical approximation being applied to I gives

$$\sigma_r(\theta,\omega) = \frac{e^2\tilde{\beta}_0\omega T\mu\sin^2\theta}{4\pi^2 c s_c\cos\theta}\cos^2\psi_c \tag{4.17}$$

for $\theta < \theta_c$ and σ_r is exponentially small outside this angular region. Here

$$s_c = (n\tilde{\beta}_0\cos\theta - 1)^{1/2}(n\tilde{\beta}_0\cos\theta - \tanh^2\frac{T_0}{T})^{1/2}, \quad \psi_c = \omega t_c - kn\cos\theta z_c + \frac{\pi}{4};$$

t_c is found from the equation

$$\cosh\frac{2t_c}{T} = \tilde{\beta}_0 n\cos\theta(1+\cosh\frac{2T_0}{T}) - \cosh\frac{2T_0}{T},$$

where $z_c = z(t_c)$, and z is given by (2.5). Unfortunately, we did not succeed to obtain the Tamm formula (1.1) from the radiation intensity (4.13). It should appear in the limit $T/T_0 \to 0$ (when the horizontal part of the charge trajectory (where $v \approx \tilde{v}_0$) is large). Equations (4.15) and (4.16) are infinite at the Cherenkov angle, but do not oscillate, contrary to the Tamm intensity (1.1). The quasiclassical expression (4.17) oscillates, but it is also infinite at the Cherenkov angle (again, contrary to the Tamm intensity).

Formerly, analytical radiation intensities for the charge motion in vacuum shown in Fig.3, were obtained in [8] and discussed in [9]. In this case, the radiation intensity at high frequencies is exponentially small for all angles.

4.4 Pure decelerated charge motion

We consider now the pure decelerated motion shown in Fig. 4. When approximations (1-3) of section 3 are fulfilled (i.e., ψ is of the form (2.3)), the integrals entering into (3.3) can be taken in a closed form [14]. Using them, we evaluate the intensity of radiation:

$$\sigma_r(\theta) = \frac{e^2k^2n\sin^2\theta}{4\pi^2 c}[(\int_{z_1}^{z_2} dz'\cos\psi_1)^2 + (\int_{z_1}^{z_2} dz'\sin\psi_1)^2] =$$

$$= \frac{e^2\sin^2\theta}{2\pi^2 cn\cos^2\theta}\{1-\cos(u_2^2-u_1^2) + \pi\alpha^2[(C_2-C_1)^2+(S_2-S_1)^2]\pm$$

$$\pm\sqrt{2\pi}\alpha[(C_2-C_1)(\sin u_2^2 - \sin u_1^2) - (S_2-S_1)(\cos u_2^2 - \cos u_1^2)]\}, \tag{4.18}$$

where

$$\alpha = \sqrt{\frac{k(z_2-z_1)}{n|\cos\theta(\beta_2^2-\beta_1^2)|}}, \quad u_1 = \sqrt{\frac{k(z_2-z_1)n|\cos\theta|}{|\beta_2^2-\beta_1^2|}}(\beta_1 - \frac{1}{n\cos\theta}),$$

$$u_2 = \sqrt{\frac{k(z_2-z_1)n|\cos\theta|}{|\beta_2^2-\beta_1^2|}}(\beta_2 - \frac{1}{n\cos\theta}), \quad \beta_1 = \frac{v_1}{c}, \quad \beta_2 = \frac{v_2}{c}.$$

Plus and minus signs in (4.18) refer to $\cos\theta > 0$ and $\cos\theta < 0$, respectively. Further, $\beta_1 = v_1/c$ and $\beta_2 = v_2/c$. When $v_1 \to v_2 = v$, the radiation intensity (4.18) goes into the Tamm formula (1.1) in which one should put $z_0 = (z_2 - z_1)/2$. Usually, the ratio of the motion interval to the observed wavelength is very large. In this case, one can change the Fresnel integrals by their asymptotic values. For the motion corresponding to $\beta_1 n > 1$ and $\beta_2 n > 1$, one finds that for $k(z_2 - z_1) >> 1$, the radiation intensity is given by

$$\sigma_r = \frac{e^2 n \sin^2\theta}{\pi^2 c}\{\frac{1}{4}[\frac{\beta_2 - \beta_1}{(1-\beta_1 n\cos\theta)(1-\beta_2 n\cos\theta)}]^2 + \\ + \frac{\beta_1\beta_2}{(1-\beta_1 n\cos\theta)(1-\beta_2 n\cos\theta)}\sin^2\psi\} \tag{4.19}$$

for $0 < \theta < \theta_2$ and $\theta > \theta_1$. Here θ_1, θ_2 and ψ are defined by

$$\cos\theta_1 = 1/\beta_1 n, \quad \cos\theta_2 = 1/\beta_2 n, \quad \psi = \frac{k(z_2 - z_1)}{\beta_1 + \beta_2}(\frac{\beta_1 + \beta_2}{2} n\cos\theta - 1).$$

On the other hand, for $\theta_2 < \theta < \theta_1$ one has

$$\sigma_r = \sigma_r(4.19) + \frac{e^2\sin^2\theta}{\pi c n\cos^2\theta}[\alpha^2 + \frac{\alpha n\cos\theta}{\sqrt{2\pi}}(\beta_2\frac{\cos 2u_2}{\beta_2 n\cos\theta - 1} - \beta_1\frac{\cos 2u_1}{\beta_1 n\cos\theta - 1})]. \tag{4.20}$$

The term proportional to α^2 is much larger than the oscillating first and last ones everywhere except for the angles close to θ_1 and θ_2. For these angles, the above expansion of Fresnel integrals fails (since u_1 and u_2 vanish at these angles). These formulae mean that the radiation intensity oscillates with decreasing amplitude for $0 < \theta < \theta_2$ and $\theta > \theta_1$, and has a plato

$$\frac{e^2\alpha^2\sin^2\theta}{\pi c n\cos^2\theta} \tag{4.21}$$

for $\theta_2 < \theta < \theta_1$. Outside this plato, the radiation intensity is $k(z_2 - z_1)$ times smaller than (4.21). Yet, it does not decrease for $k(z_2 - z_1) \to \infty$, contrary to the motions shown in Figs. 1-3. The reason is that motion shown in Fig. 4 is "more discontinuous" relative to the ones shown in Figs. 1-3. Indeed, Figs. 2 and 3 correspond to the absolutely continuous motions and their radiation intensities decrease exponentially in the angular region $\theta > \theta_c$ for $\omega \to \infty$. There are no velocity jumps for the motion shown in Fig.1, but the accelerations are discontinuous at the start and end of motion and at the moments when the uniform motion meets the acelerated (or decelerated) one. Correspondingly, the radiation intensity decreases like $1/k(z_0 - z_1)$ for $\theta > \theta_c$. For the motion shown in Fig. 4, both velocity and and acceleration are discontinuous at the start and end of motion. The corresponding radiation intensity does not decrease outside the plato for $k(z_2 - z_1) \to \infty$ although it is much smaller than its value at the plato (4.21).

For $\beta_2 = 1/n$, the above formulae predict intensity oscillations for $\theta > \theta_1$ and their absence for $\theta < \theta_1$. Experimentally, the charge motion with deceleration is realized in Cherenkov experiments with heavy ions [17] where the energy losses are essential due to their large atomic numbers.

A particular interesting case having numerous practical applications corresponds to the complete termination of motion ($\beta_2 = 0$) . In this case, for $\beta_1 n > 1$ one gets

$$\sigma_r = \frac{e^2 n \beta_1^2}{4\pi^2 c} \frac{\sin^2\theta}{(1-\beta_1 n \cos\theta)^2} \tag{4.22}$$

for $\theta > \theta_1$ and

$$\sigma_r = \sigma_r(4.22) + \frac{e^2 \sin^2\theta}{\pi c n \cos^2\theta}[\alpha^2 - \alpha \frac{\beta_1 n \cos\theta}{\sqrt{2\pi}} \frac{\cos 2u_1}{\beta_1 n \cos\theta - 1}] \tag{4.23}$$

for $\theta < \theta_1$. Here

$$\alpha = \frac{1}{\beta_1}\sqrt{\frac{k(z_2-z_1)}{n\cos\theta}}, \quad u_1 = \sqrt{k(z_2-z_1)n\cos\theta}(1 - \frac{1}{\beta_1 n \cos\theta}).$$

Since $\alpha >> 1$, the radiation intensity for $\theta > \theta_1$ is much smaller than for $\theta < \theta_1$. There are no intensity oscillations for $\theta > \theta_1$ and there are are very small oscillations for $\theta < \theta_1$ (they are due to the term proportional α in (4.23) which is much smaller than the term proportional α^2).
When $\beta_1 n < 1$, the same Eq. (4.22) is valid for all angles. In this case, integration over the solid angle can be done analytically:

$$\sigma_r(\omega) = \int \sigma_r(\theta,\omega)d\Omega = \frac{2e^2}{\pi c n}(\frac{1}{2\beta_1 n} \ln\frac{1+\beta_1 n}{1-\beta_1 n} - 1). \tag{4.24}$$

This expression is not valid for β_1 close to $1/n$.
The singularites occurring in (4.19),(4.20),(4.22) and (4.23) are due to the condition $k(z_2 - z_1) >> 1$ used. The initial radiation intensity (4.18) is finite both for $\cos\theta = 1/\beta_1 n$ and $\cos\theta = 1/\beta_2 n$. The above considerations about the decreasing of radiation intensities at high frequencies are also applicable also to (4.22) and (4.23).

Formerly, in the time representation, the electromagnetic field of a charge moving non-uniformly in medium was obtained in [16]. Space-time propagation of the shock wave complex mentioned in the subsection (4.1) was studied there. In the spectral representation, the decelerated charge motion with the velocity change small compared with the velocity itself was studied in [11, 18]. Radiation intensities evaluated there had also plato in the neighbourhood of the Cherenkov angle.

4.5 Smooth infinite charge motion

For the motion shown in Fig. 5, one obtains

$$I = \frac{ct_0}{2n\cos\theta} \exp[\frac{1}{2} i\omega t_0 n(\beta_1 - \beta_2)\cos\theta] \frac{\Gamma(\alpha_2)\Gamma(-\alpha_1)}{\Gamma[i\omega t_0 n \cos\theta(\beta_2 - \beta_1)/2]},$$

where

$$\alpha_1 = i\omega t_0(1 - n\beta_1 \cos\theta)/2, \quad \alpha_2 = i\omega t_0(1 - n\beta_2 \cos\theta)/2.$$

Correspondingly,

$$|I|^2 = \frac{c^2 t_0 \pi(\beta_2 - \beta_1)}{2\omega n \cos\theta(1 - n\beta_1 \cos\theta)(1 - n\beta_2 \cos\theta)} \times$$

$$\frac{\sinh[\pi n \cos\theta \omega t_0(\beta_2 - \beta_1)/2]}{\sinh[\pi(1 - \beta_1 n \cos\theta)\omega t_0/2] \sinh[\pi(1 - \beta_2 n \cos\theta)\omega t_0/2]}$$

and

$$\sigma_r(\theta, \omega) = \frac{e^2 \mu \omega t_0 \sin^2\theta}{8\pi c \cos\theta} F, \tag{4.25}$$

where

$$F = \frac{(\beta_2 - \beta_1)}{(1 - n\beta_1 \cos\theta)(1 - n\beta_2 \cos\theta)} \times$$

$$\frac{\sinh[\pi n \cos\theta \omega t_0(\beta_2 - \beta_1)/2]}{\sinh[\pi(1 - \beta_1 n \cos\theta)\omega t_0/2] \sinh[\pi(1 - \beta_2 n \cos\theta)\omega t_0/2]}.$$

We put $\cos\theta_1 = 1/\beta_1 n$ and $\cos\theta_2 = 1/\beta_2 n$. Consider the behaviour of the radiation intensity for $\omega t_0 >> 1$. Obviously, $\theta_1 < \theta_2$ for the decelerated motion ($\beta_2 > \beta_1$). Let $\beta_1 n > 1$ and $\beta_2 n > 1$. Then, for $\theta < \theta_1$

$$F = \frac{2(\beta_2 - \beta_1)}{(\beta_1 n \cos\theta - 1)(\beta_2 n \cos\theta - 1)} \exp[-\pi\omega t_0(\beta_1 n \cos\theta - 1)]. \tag{4.26}$$

For $\theta > \theta_2$

$$F = \frac{2(\beta_2 - \beta_1)}{(\beta_1 n \cos\theta - 1)(\beta_2 n \cos\theta - 1)} \exp[-\pi\omega t_0(1 - \beta_2 n \cos\theta)]. \tag{4.27}$$

Finally, for $\theta_1 < \theta < \theta_2$

$$F = \frac{2(\beta_2 - \beta_1)}{(1 - \beta_1 n \cos\theta)(\beta_2 n \cos\theta - 1)}. \tag{4.28}$$

We see that two maxima should be observed at Cherenkov angles θ_1 and θ_2. Between these maxima, the radiation intensity is a smooth function of θ. For $\theta < \theta_1$ and $\theta > \theta_2$, the radiation intensity is exponentially small.
For $\beta_1 n < 1$ and $\beta_2 n > 1$, F equals (4.28) for $0 < \theta < \theta_2$, and (4.27) for $\theta > \theta_2$.
For $\beta_1 n < 1$ and $\beta_2 n < 1$, F has the form (4.27) and the radiation intensity is exponentially small for all angles.

For $\omega t_0 << 1$ (this corresponds either to the sharp change of the charge velocity near $t = 0$ or to large observed wavelengths) one finds

$$\sigma_r(\theta, \omega) = \frac{e^2 n \mu \sin^2\theta}{4\pi c} \frac{(\beta_2 - \beta_1)^2}{(1 - \beta_1 n \cos\theta)^2 (1 - \beta_2 n \cos\theta)^2}. \tag{4.29}$$

In this case, $\sigma_r(\theta,\omega)$ has two maxima at the Cherenkov angles θ_1 and θ_2, if both $\beta_1 n > 1$ and $\beta_2 n > 1$ and one maximum at θ_2 if $\beta_1 n < 1$ and $\beta_2 n > 1$.

Strictly speaking, the validity of Eqs. (4.25)-(4.29) is slightly in doubt. When obtaining them, we used Eq. (3.5) the validity of which implies that a charge motion takes place on the interval much smaller than the radius of the observation sphere S. However, Eq. (2.14) describes the unbounded charge motion. For the sufficiently large time, when a charge will be outside S, the validity of (3.5) will be violated.

Formerly, analytical radiation intensities for the charge motion in vacuum shown in Fig.5, were obtained in [10] and discussed in [9]. In this case, the radiation intensity at high frequencies is exponentially small for all angles.

5 Numerical results

In Fig. 7, the radiation intensities $\sigma_r(\theta,\omega) = d^2\mathcal{E}/d\omega d\Omega$ corresponding to Fig. 1, are compared with the Tamm intensities (1.1) evaluated for the same β_0, L and λ. The parameter x_a is the ratio of the path on which a charge moves non-uniformly to the total path. For example, $x_a = 0.01$ means that a charge moves non-uniformly on the 1/100 part of the total path. It is seen that for rather moderate acceleration paths ($x_a = 0.1$ and $x_a = .01$), the radiation intensities σ_r fall rapidly for $\theta > \theta_c$. For smaller x_a, σ_r and σ_T approach each other (Fig. 7, c, d). The radiation intensity (3.3), with analytical I defined by (4.1)-(4.3), covers the whole angular region. The approximated formula (4.5), valid for $kx_a >> 1$, describes the radiation intensity for $\theta < \theta_c$. The oscillations of σ_r are due to the factor $(1 + \sin 2\gamma)$ in (4.5).

Radiation intensities $\sigma_r(\theta)$ corresponding to the charge motion of Fig.2 are presented in Fig. 8 for a number of $\beta_0 = v_0/c$ together with the Tamm intensities σ_T corresponding to the same L, β_0 and λ. It is seen that the positions of main maxima of σ_r and σ_T coincide for $\beta_0 > c_n$ and are at the Cherenkov angle defined by $\cos\theta_c = 1/\beta_0 n$. For $\beta_0 < c_n$, σ_r is much smaller than σ_T (d). For $\theta > \theta_c$, σ_r falls very rapidly and σ_T dominates in this angular region (a,b,c). For $\theta < \theta_c$, σ_r is much larger than σ_T (a,b). This is in complete agreement with analytical results of subsection (4.2) which predict the exponential decreasing of σ_r for $\theta > \theta_c$ and its oscillations described by (4.11) for $\theta < \theta_c$.

Radiation intensities $\sigma_r(\theta)$ corresponding to Fig. 3, for fixed $\beta_0 = 1$, $L = 0.1cm$, $\lambda = 4 \cdot 10^{-5} cm$ and a number of diffuseness parameters $\tau_0 = T_0/T$, are shown in Fig. 9. The positions of main maxima are at the Cherenkov angle θ_c. The fast angular oscillations in the $\theta < \theta_c$ region are described by the quasiclassical formula (4.17). Again we observe that σ_r falls almost instantly for $\theta > \theta_c$. The reason for this is due to different asymptotics of radiation intensities which fall exponentially for the absolutely continuous motion presented in Fig. 3 and do not decrease with frequency (except for $\cos\theta = 1/\beta n$) for the original Tamm problem involving two velocity jumps. Much larger values of τ_0, than the ones presented in Fig.9, are needed to match these angular intensities.

Radiation intensities for $\beta_1 n > 1$ and $\beta_2 n > 1$ corresponding to Fig. 4 are shown in Fig. 10. In accordance with (4.21), σ_r is almost constant in the angular interval $\theta_2 < \theta < \theta_1$. Outside it, the angular asymptotic behaviour of σ_r is the same as the σ_T one. The reason for this is that the motion corresponding to Fig.4 has the same discontinuities as the original Tamm problem one (two velocity jumps at the start and end of motion).

An important case is the decelerated motion with a final zero velocity. Experimentally, it is realized in heavy water reactors where electrons arising in β decay are decelerated up to their complete stopping, in neutrino experiments, in the original Cherenkov experiments, etc. Radiation intensities for different initial velocities are shown in Fig. 11. It is easy to check that their maxima, despite the highly non-uniform character of this motiom, are always at the Cherenkov angle θ_1 defined by $\cos\theta_1 = 1/\beta_1 n$ and corresponding to the initial velocity v_1. Analytically, these radiation intensities are described by Eq.(4.18) in the whole angular interval. Its approximated versions (4.22) and (4.23), valid for $kL >> 1$, describe radiation intensities in the angular intervals $\theta > \theta_1$ and $0 < \theta < \theta_1$, resp. For the treated motion, both the velocity and acceleration exhibit jumps at the beginning of motion and only the acceleration is discontinuous at its end. Therefore, the decrease of the radiation intensity is not so pronounced as for absolutely continuous motions shown in Figs. 2 and 3 and for the motion without velocity jumps shown in Fig. 1.

An important quantity is the total energy radiated per unit frequency. It is obtained by integration of the angular-frequency distribution over the solid angle:

$$\sigma_r(\omega) = \frac{d\mathcal{E}}{d\omega} = \int \sigma_r(\omega, \theta) d\Omega. \tag{5.1}$$

The integration of the Tamm intensity (1.1) over the solid angle gives the frequency distribution of the radiated energy $\sigma(\omega)$. Explicitly, it was written out in [12]. Since it is rather complicated, we do not give it here denoting it by $\sigma([12])$. In the limit $\omega t_0 \to \infty$, it is transformed into the following expression given by Tamm [1]:

$$\sigma_T(\omega) = \frac{e^2 kL}{c}(1 - \frac{1}{\beta_n^2})\Theta(\beta n - 1) + \frac{4e^2}{\pi cn}(\frac{1}{2\beta_n} \ln \frac{1+\beta_n}{|\beta_n - 1|} - 1). \tag{5.2}$$

Here $k = \omega/c$, $\beta_n = \beta n$, and $L = 2z_0$ is the motion interval. Equation (5.2) has a singularity at $\beta = 1/n$, while $\sigma([12])$ is not singular there. To see how they agree with each other, we present them and their difference (Fig. 12) as a function of the velocity β for the parameters $L = 2z_0 = 0.1cm$ and $\lambda = 4 \cdot 10^{-5} cm$ used above. It is seen that they coincide with each other everywhere except for the closest vicinity of $\beta = 1/n$.

We integrate now angular distributions corresponding to the decelerated motion with a final zero velocity and shown in Fig. 11, and relate them to the Tamm integral intensitiy (5.2). Fig. 13 demonstrates that, despite their quite different angular distributions, the ratio R of these integral intensities does not depend on the

frequency except for the neighbourhood of $\beta = 1/n$ where (5.2) is not valid. For the charge velocity v above the light velocity in medium c_n (where the Tamm intensity is approximately proportional to ω), this ratio decreases as v approaches c_n. For $v < c_n$ (where the ω dependence given by the Tamm formula is logarithmic), R begins to rise. Since the radiation intensity (4.24) is one half of $\sigma_T(\omega)$ for $\beta_1 n < 1$, R tends to 1/2 for small β_1 (Eq. (4.24) is not valid for $\beta_1 n \approx 1$). We see that the integral intensities for the decelerated motion, up to a factor independent of ω, coincide with the Tamm one. Therefore, the total energy for the decelerated motion

$$\mathcal{E} = \int_{\omega_1}^{\omega_2} d\omega \frac{d\mathcal{E}}{d\omega}$$

radiated in the frequency interval (ω_1, ω_2) up to the same factor coincides with the Tamm integral intensity.

Tamm [1] obtained the following condition

$$\frac{t_0^2}{2} \left| \frac{dv}{dt} \right| << \lambda \tag{5.3}$$

for the frequency spectrum $\sigma(\omega)$ to be the linear function of frequency. For the treated decelerated motion, this condition takes the form

$$\frac{v_1 - v_2}{v_1 + v_2} << \frac{\lambda}{L}, \tag{5.4}$$

where $L = z_2 - z_1$ is the motion interval. When the final velocity is zero, (5.4) is reduced to $L << \lambda$, which for $L = 0.1$ and a particular $\lambda = 4 \cdot 10^{-5}$ takes the form $1 << 4 \cdot 10^{-4}$. Figure 13 demonstrates that the frequency independence of the above ratio R takes place despite the strong violation of the Tamm condition (5.3).

6 Discussion and Conclusion

We have considered a number of the smoothed Tamm problem versions allowing analytical solutions. They have a common property that for the charge velocity greater than the light velocity in medium, the angular region exists where the radiation intensity is proportional to the frequency and the one where the radiation intensity is small for high frequencies.

This investigation is partly inspired by the influential paper [19], where the charge motion with the velocity linearly decreasing with time was investigated. Numerical radiation intensities obtained there, strongly resemble our analytical ones (4.19)-(4.21). In addition, the authors of [19] correctly guessed that the Tamm radiation intensity (1.1) is related to the velocity jumps at the start and end of motion. Our understanding of this problem coincides with that given in [7-10] for the charge motion in vacuum where it was shown that radiation intensities for the absolutely

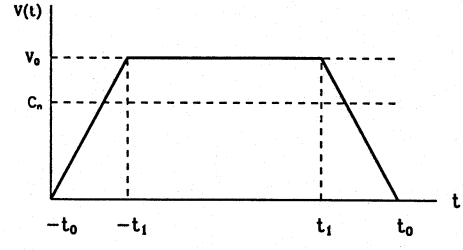

Figure 1: Superposition of accelerated ($-t_0 < t < -t_1$), uniform ($-t_1 < t < t_1$), and decelerated ($t_1 < t < t_0$) motions. The drawback of this motion is due to the acceleration jumps at $t = \pm t_0$ and $t = \pm t_1$.

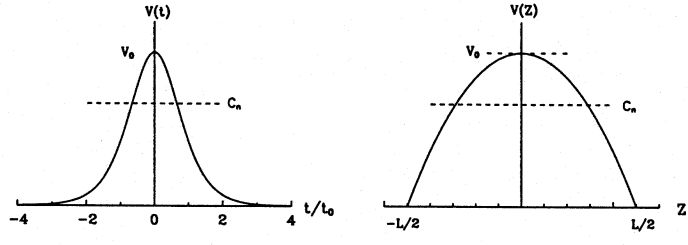

Figure 2: The motion corresponding to (2.1). Left and right parts correspond to $v(t)$ and $v(z)$ where z is the charge position at the time t. It is seen that the charge position is confined to a finite space interval $(-L/2, L/2)$.

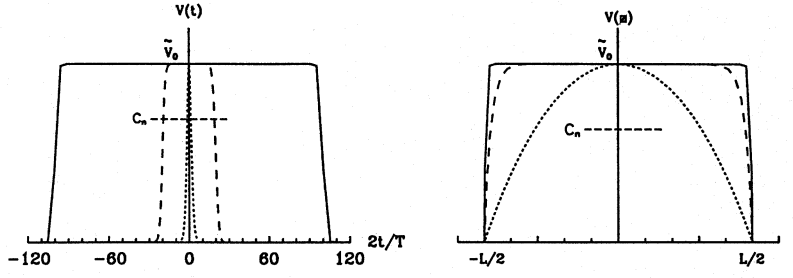

Figure 3: The motion corresponding to (2.3). Dotted, broken and dotted lines correspond to $\tau_0 = T_0/T = 0.5,\quad 10$ and 25, resp. For large τ_0, the interval where a charge moves with almost constant velocity increases. The charge position is confined to a finite space interval $(-L/2, L/2)$. This motion is much richer than the one shown in Fig.2.

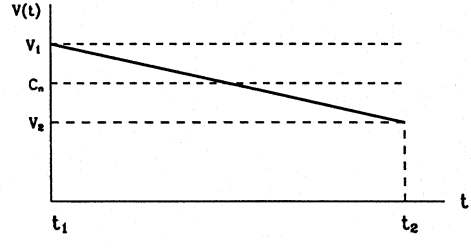

Figure 4: Charge motion with a constant deceleration treated in the text.

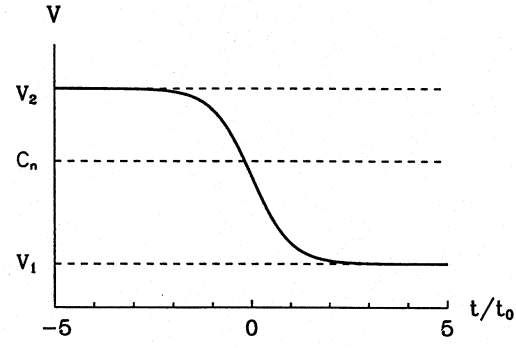

Figure 5: The unbounded charge motion corresponding to (2.14) and describing the smooth transition from the velocity v_2 at $t = -\infty$ to the velocity v_1 at $t = \infty$.

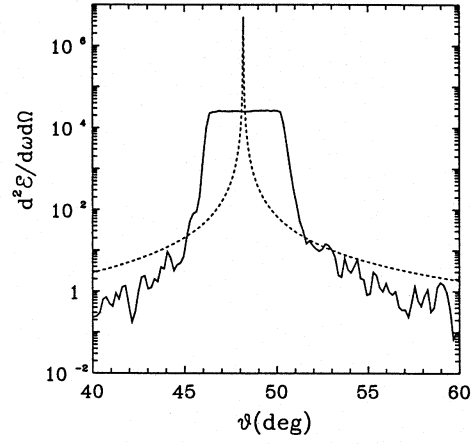

Figure 6: Angular radiation intensities (in units e^2/c) corresponding to the charge motion in a finite interval (Tamm problem). The solid and dotted lines correspond to the radii of the observation sphere $r = 1cm$ and $r = \infty$. The latter intensity is described by the Tamm formula (1.1). The original angular intensities are highly oscillating functions. To make them more visible, we draw the Tamm intensity (1.1) (dotted curve) through its maxima. Other intensities, for which the maxima positions are not explicitly known, are obtained by averaging over three neighbouring points, thus, considerably smoothing the oscillations. This is valid for the subsequent Figs. 7-10. The charge velocity is $\beta_0 = 1$, the motion interval $L = 0.1cm$, the wavelength $\lambda = 4 \cdot 10^{-5}cm$, the refractive index $n = 1.5$. The last three parameters are the same for all figures.

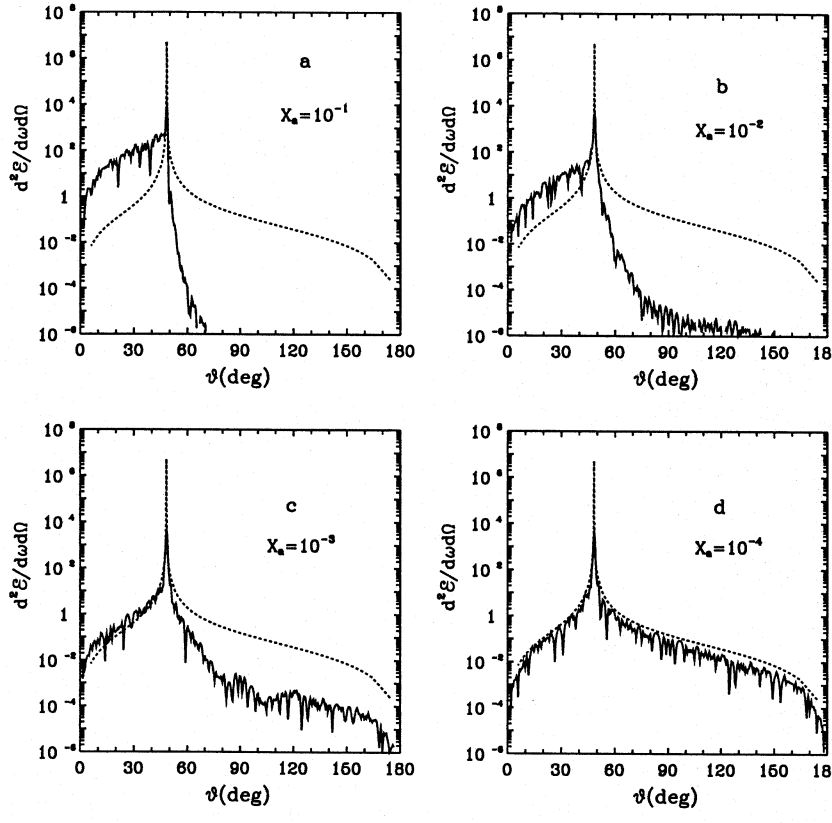

Figure 7: Angular radiation intensities (solid curves) corresponding to the charge motion shown in Fig. 1 for $\beta_0 = 1$ and a number of non-uniform motion lengths x_a. Here x_a is the ratio of the path where a charge moves non-uniformly to the total path. It is seen that angular radiation intensities approach the Tamm one (dotted curves) when $x_a \to 0$.

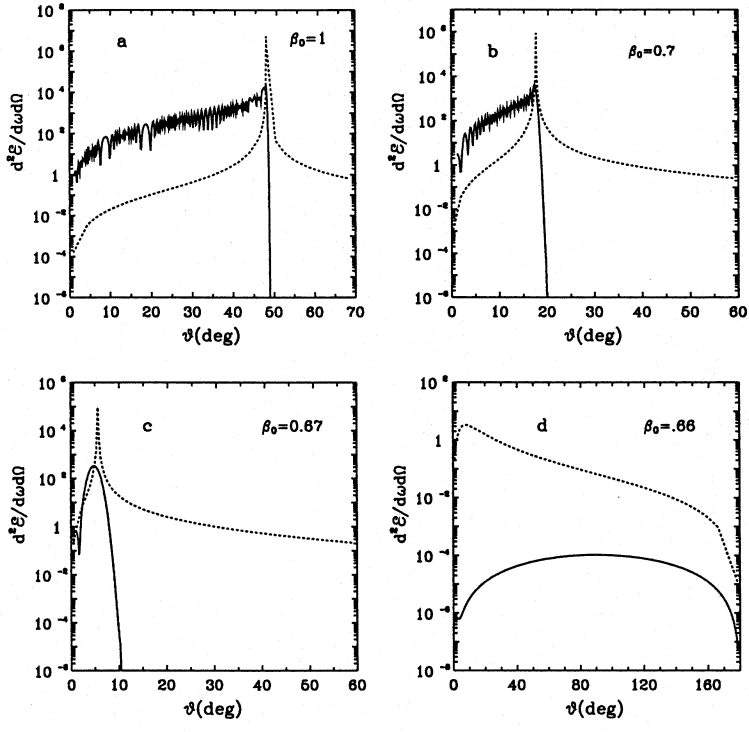

Figure 8: Angular radiation intensities corresponding to the charge motion shown in Fig. 2 (solid curves) and the Tamm intensities (dotted lines) for a number of v_0. For $v_0 > c_n$, the maximum of intensity is at the Cherenkov angle θ_c defined by $\cos\theta_c = 1/\beta_0 n$. The angle θ_c decreases with decreasing v_0. For $\theta > \theta_c$ and $\beta_0 > 1/n$, the radiation intensity falls almost instantly. For $\beta_0 < 1/n$, the radiation intensity is exponentially small for all angles. This is explained analytically in section 4.

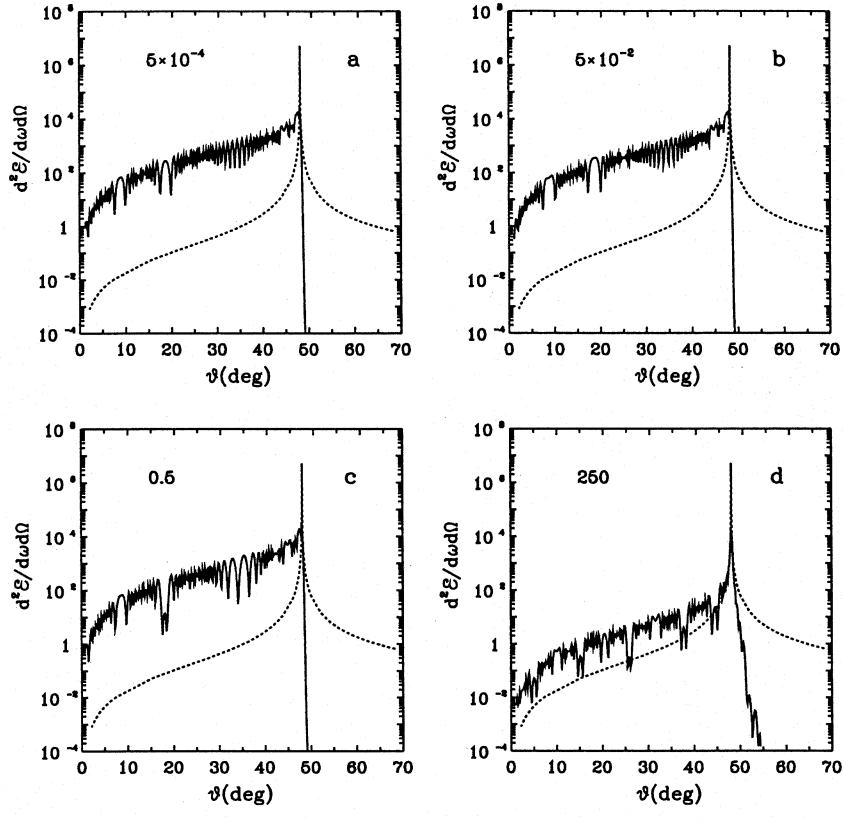

Figure 9: Angular radiation intensities corresponding to the charge motion shown in Fig. 3 (solid lines) for $\tilde{\beta}_0 = 1$ and a number of diffuseness parameters $\tau_0 = T_0/T$. Angular intensities approach the Tamm one (dotted line) rather slowly even for large values of τ_0. This is due to their different asymptotic behaviour.

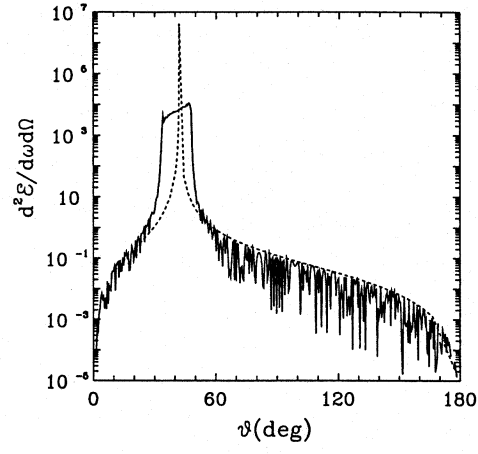

Figure 10: Angular radiation intensity corresponding to Fig.4 for $\beta_1 = 1$ and $\beta_2 = 0.8$ greater than $1/n$. The plato in the angular region $\theta_2 < \theta < \theta_1$ is described by (4.21). Outside this plato, the asymptotics of σ_r and σ_T are the same.

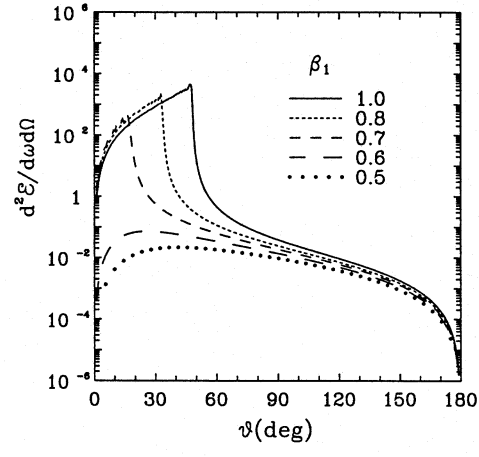

Figure 11: Angular radiation intensities corresponding to the charge motion with complete stopping for a number of initial velocities β_1. It is seen that these intensities do not oscillate. The angle where they are maximal increases with increase of β_1.

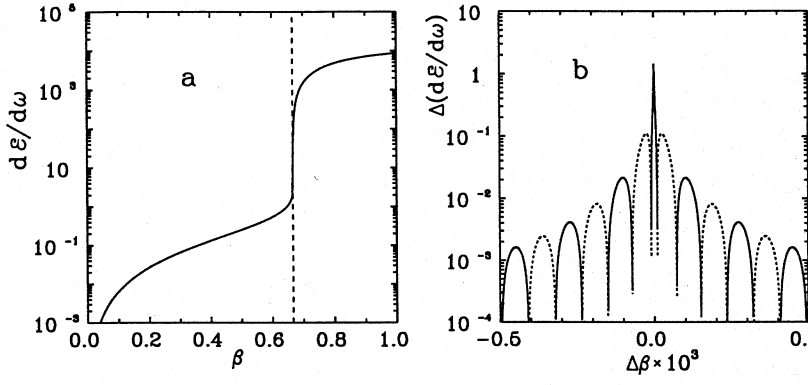

Figure 12: (a) Frequency distributions of the radiated energy (in e^2/c units) obtained in [12] and its simplified version (5.2) as functions of the charge velocity. They are indistinguishable in this scale; (b) the difference between (5.2) and σ_r([12]). The regions where this difference is negative are shown by dotted lines; $\Delta\beta$ means $\beta - 1/n$.

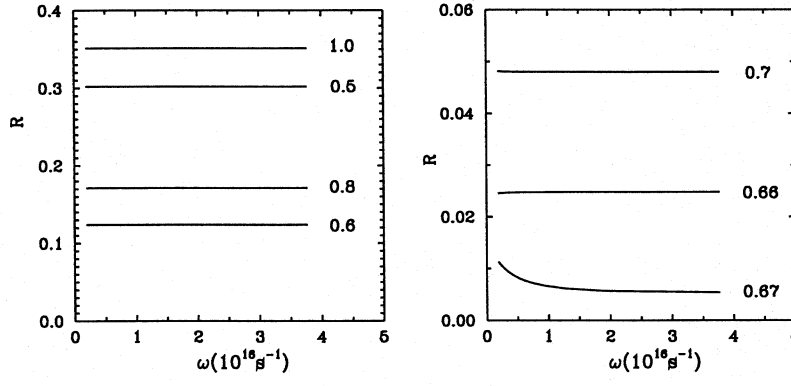

Figure 13: The ratio R of the integral intensity for the motion with a zero final velocity to the Tamm integral intensity (5.2) for a number of initial velocities v_1. Although R does not depend on the frequency (except for the velocity $\beta_1 = 0.67$ close to the Cherenkov threshold $1/n$), it strongly depends on β_1 being minimal at the threshold. Analytical formula (4.24) shows that $R \to 0.5$ for small β_1. To this frequency interval there corresponds the wavelength interval ($5 \cdot 10^{-6} cm < \lambda < 10^{-4} cm$) which encompasses the visible light interval ($4 \cdot 10^{-5} cm < \lambda < 8 \cdot 10^{-5} cm$). Numbers at curves mean β_1.

continuous motion are the exponentially decreasing functions of ω. The modification for the charge moving in medium looks as follows. The asymptotic behaviour of the radiation intensity depends on the fact how much the charge motion is discontinuous. For example, for the absolutely continuous charge motions shown in Figs. 2, 3 and 5, the radiation intensities decrease exponentially with ω for θ above some critical angle θ_c, and are proportional to ω for $\theta < \theta_c$. For the motion without velocity jumps (but with the acceleration ones) shown in Fig.1, the radiation intensity falls like $1/\omega$ for $\theta > \theta_c$ and is proportional to ω for $\theta < \theta_c$. For the charge motion with velocity and acceleration jumps shown in Fig. 4, the radiation intensity does not depend on the frequency for $\theta > \theta_c$, although it is much smaller than for $\theta < \theta_c$ (again, in this angular region, σ_r is proportional to ω).

A question arises what kind of the radiation fills the angular region $\theta < \theta_c$ (see Figs. 7(a,b), 8(a,b), 9 and 11). For this, we again turn to Refs. [15, 16] where the exact radiation fields were obtained for the charge accelerated and decelerated motions. At the start of motion ($t = 0$), the spherically symmetric Bremsstrahlung shock wave (BSW) arises which propagates with the light velocity in medium. At the moment t_0, when the charge velocity coincides with the charge velocity in medium, a complex arises consisting of the finite Cherenkov shock wave SW1 and the shock wave SW2 closing the Cherenkov cone. The singularities carried by these two shock waves are the same and are much stronger than the singularity carried by BSW (for details see [15, 16]). The SW1, attached to a moving charge, intersects the motion axis at the angle $\pi/2 - \theta_{Ch}$, where θ_{Ch} is the Cherenkov angle corresponding to the current charge velocity ($\cos\theta_{Ch} = 1/\beta n$). Obviously, $\theta_{Ch} = 0$ at $t = t_0$ and $\theta_{Ch} = \theta_c$ at the end of acceleration. Here θ_c is the Cherenkov angle corresponding to the maximal charge velocity. The SW2, detached from a charge and intersecting the motion axis behind the charge at the right angle, differs from zero in the angular sector $0 < \theta < \theta_{Ch}$. The angular distribution in the spectral representation (since transition to it involves integration over all times) fills the angular region $0 < \theta < \theta_c$. We conclude: The radiation intensity in the $0 < \theta < \theta_c$ angular region consists of the Cherenkov shock wave, the one closing the Cherenkov cone and the Bremsstrahlung shock wave.

References

[1] Tamm I.E., 1939, J.Phys. USSR, 1, 439.

[2] Vavilov S.I., 1934, Dokl. Akad, Nauk, 2, 8, 457.

[3] Zrelov V.P., Ruzicka J., 1989, Chech.J.Phys. B, 39, 368.

[4] Zrelov V.P., Ruzicka J., 1992, Chech.J.Phys., 42, 45.

[5] Lukyanov V.K., Eldyshev Yu.N. and Pol' Yu.S., 1973, Sov. J. Nucl. Phys., 16, 282.

[6] Grypeos M.E., Koutroulos G., Lukyanov V.K. and Shebeko A.V., 2001, Particles and Nuclei, 32, 1494.

[7] Abbasov I.I., 1982, Kratkije soobchenija po fizike FIAN, No 1, 31.

[8] Abbasov I.I., 1985, Kratkije soobchenija po fizike FIAN, No 8, 33.

[9] Abbasov I.I., Bolotovskii B.M. and Davydov V.A., 1986, Usp. Fiz. Nauk, 149, 709.

[10] Bolotovskii B.M. and Davydov V.A., 1981, Izv. Vuzov, Radiofizika, No 1, 31.

[11] Afanasiev G.N. and Shilov V.M., 2000, J. Phys.D, 33, 2931.

[12] Afanasiev G.N., Kartavenko V.G. and Ruzicka J., 2000, J. Phys. A, 33, 7585.

[13] Afanasiev G.N., Kartavenko V.G. and Stepanovsky Yu.P., 1999, 1999, J. Phys.D, 32, 2029.

[14] Afanasiev G.N. and Shilov V.M., 2002, JINR Preprint E2-2002-36

[15] Afanasiev G.N. and Shilov V.M., 2000, Physica Scripta, 62, 326.

[16] Afanasiev G.N., Eliseev S.M. and Stepanovsky Yu.P., 1998, Proc. Roy. Soc. Lond. A, 454, 1049; Afanasiev G.N. and Kartavenko V.G., 1999, Can. J. Phys., 77, 561.

[17] Ruzicka J. et al., 2000, Nucl. Instr. Methods,A, 431, 148.

[18] Kuzmin E.S. and Tarasov A.V., 1993, JINR Rapid Communications, 4[61]-93, 64, Dubna, 1993.

[19] Krupa L., Ruzicka J. and Zrelov V.P., 1995, JINR Preprint P2-95-281, Dubna, 1995

Received on May 17, 2002.

Макет *Т. Е. Попеко*

ЛР № 020579 от 23.06.97.
Подписано в печать 20.06.2002.
Формат 60 × 90/16. Бумага офсетная. Печать офсетная.
Усл. печ. л. 1,93. Уч.-изд. л. 3,67. Тираж 425 экз. Заказ № 53366.

Издательский отдел Объединенного института ядерных исследований
141980, г. Дубна, Московская обл., ул. Жолио-Кюри, 6.